Multi-nanolayered VO2/Sapphire Thin Film via Spinodal Decomposition

Sun, G.Y.; Cao, X.; Yue, Yuanzheng; Gao, X.; Long, S.W.; Li, N.; Li, R.; Luo, H.J.; Jin, P.

Published in:
Scientific Reports

DOI (link to publication from Publisher):
10.1038/s41598-018-23412-4

Publication date:
2018

Document Version
Publisher's PDF, also known as Version of record

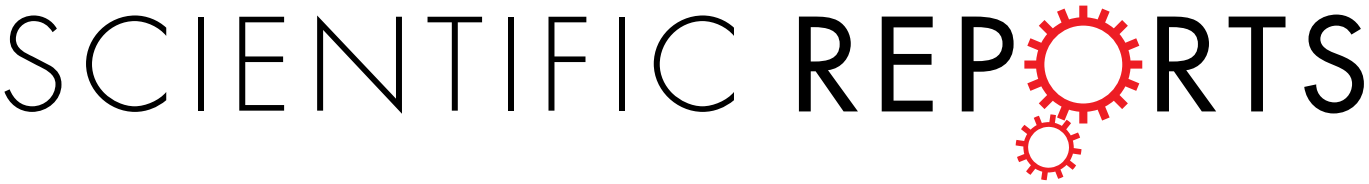

OPEN

Multi-nanolayered VO_2/Sapphire Thin Film *via* Spinodal Decomposition

Received: 29 December 2017
Accepted: 9 February 2018
Published online: 28 March 2018

Guangyao Sun[1,2], Xun Cao[1], Yuanzheng Yue[3,4], Xiang Gao[5], Shiwei Long[1,2], Ning Li[1,6], Rong Li[1], Hongjie Luo[7] & Ping Jin[1,8]

Coating of VO_2-based thin film has been extensively studied for fabricating energy-saving smart windows. One of the most efficient ways for fabricating high performance films is to create multi-nanolayered structure. However, it has been highly challenge to make such layers in the VO_2-based films using conventional methods. In this work, a facile two-step approach is established to fabricate multilayered VO_2-TiO_2 thin films. We first deposited the amorphous thin films upon sputtering, and then anneal them to transform the amorphous phase into alternating Ti- and V-rich multilayered nanostructure via a spinodal decomposition mechanism. In particular, we take advantage of different sapphire substrate planes (A-plane (11–20), R-plane (1–102), C-plane (0001), and M-plane (10-10)) to achieve different decomposition modes. The new approach has made it possible to tailoring the microstructure of the thin films for optimized performances by controlling the disorder-order transition in terms of both kinetic and thermodynamic aspects. The derived thin films exhibit superior optical modulation upon phase transition, significantly reduced transition temperature and hysteresis loop width, and high degradation resistance, these improvements indicate a high potential to be used for fabricating the next generation of energy saving smart windows.

There has been a long-standing demand for nanoscale phase separation owing to its connection to material functionalities. In recent years, intensive efforts have been devoted to understanding the connection[1–4], and varied approaches for creating functional thin films have been reported, e.g., DNA-mediated self-assembly[5], feedback-driven self-assembly[6], and electrochemical techniques[7]. Conventional methods for fabricating thin films usually involve procedures such as template intermediates and/or post treatments, which make the fabrication process complicated and hence unstable. Self-assembly *via* spinodal decomposition is a promising solution since spinodal decomposition has proven to be efficient in controlling structural features at nanoscale[8–10]. The spinodal decomposition is a mechanism for the rapid decomposition of one thermodynamically stable mixture of liquids or solids into two coexisting phases[11]. In contrast to a nucleation-growth process that results in a random mixture of the two, spinodal decomposition is characterized by long-range spatial correlation, quasi-periodicity, and self-organization with a nearly sinusoidal composition modulation[12]. The structure with compositional fluctuations formed by spinodal decomposition tend to form at nanometer scale[13]. Thus, spinodal decomposition provides a practical route to produce a finely dispersed microstructure that can significantly enhance the material properties.

Most two-phase spinodal systems are consist of two phases with similar crystal structures and physical properties, e.g., metallic alloys[11], SnO_2-TiO_2 system[14–16], Al_2O_3-Cr_2O_3 system[17] and AlN-SiC system[18]. This similarity

[1]State Key Laboratory of High Performance Ceramics and Superfine Microstructure, Shanghai institute of Ceramics, Chinese Academy of Sciences, Dingxi 1295, Changning, Shanghai, 200050, China. [2]University of Chinese Academy of Sciences, Beijing, 100049, China. [3]Section of Chemistry, Aalborg University, DK-9220, Aalborg, Denmark. [4]State Key Laboratory of Silicate Materials for Architectures, Wuhan University of Technology, Wuhan, 430070, China. [5]Thin Films and Nanostructures Group, Materials Science and Technology Division, Oak Ridge National Laboratory, 1 Bethel Valley Rd., Oak Ridge, Tennessee, 37831, USA. [6]Department of Materials Science and Engineering, College of science, China University of Petroleum Beijing, No. 18 Fuxue RD, Beijing, 102249, China. [7]School of Materials Science and Engineering, Shanghai University, 99 Shangda Road, Shanghai, 200444, China. [8]Materials Research Institute for Sustainable Development, National Institute of Advanced Industrial Science and Technology, Nagoya, 463-8560, Japan. Guangyao Sun and Xun Cao contributed equally to this work. Correspondence and requests for materials should be addressed to X.C. (email: caoxun2015@gmail.com) or P.J. (email: p-jin@mail.sic.ac.cn)

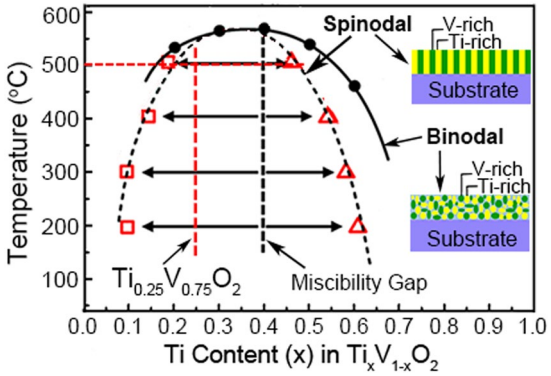

Figure 1. Phase diagram of the VO_2-TiO_2 system. Reprinted (adapted) with permission from (Z. Hiroi, *et al.* Spinodal Decomposition in the TiO_2-VO_2 System. *Chem. Mater.* **25**, 2202–2210 (2013). Copyright (2013) American Chemical Society.

limits the functionality of many decomposed systems. Spinodal decomposition of the TiO_2/VO_2 (TVO) system, which was discovered by Zanma and Ueda in 1998 and recently investigated in bulk materials by Z. Hiroi *et al.*[19,20], is of great interest because of its unique properties of the two components (TiO_2 and VO_2). VO_2 is a crucial component for achieving multi-functionalities of thin film since reversible first-order semiconductor-metal phase transition is accompanied by a drastic change in the optical, electrical, and magnetic properties between its two phases[21–24]. TiO_2 is a commonly used wide band gap insulator and acts as an antireflection compound for VO_2 to increase the transmittance of a thin film in both visible and infrared regions[25–27]. Therefore, transparent TVO thin films provide an attracting application in smart windows, that is, windows that capable of regulating solar/heat transmission for energy efficiency and comfort[28]. With the advantages of simple structure, automatic control without the use of switching devices, a new approach to enable large-scale producing TVO smart windows at a lower cost is highly desired.

Our previous work[29] has shown the feasibility of spinodal decomposition on TVO thin films. However, the mechanism of spinodal decomposition in TVO system has not been fully uncovered, the decomposition-microstructure-property relation has not been explored. In the present work, TVO thin films with spinodal structures by performing room temperature sputtering-annealing are prepared using various sapphire substrates (A-plane, R-plane, C-plane and M-plane). We explore the decomposition-microstructure-property relation, reveal the mechanism of spinodal decomposition in TVO system, and we estimate the practical value of all the spinodal structures in smart window area. Our work provides an accurate self-assembled route to fabricate and control VO_2-based multilayered thin films.

Results and Discussion

Samples are abbreviated as A-A, A-R, A-C, A-M for amorphous TVO on A-plane (11–20) sapphire, R-plane (1–102) sapphire, C-plane (0001) sapphire, M-plane (10-10) sapphire substrates respectively. Representative spinodal decomposition samples on different sapphire substrates were abbreviated as SD-A, SD-R, SD-C, SD-M, and crystalline solid solution TVO on the previously mentioned sapphire substrates were abbreviated as C-A, C-R, C-C, C-M. Single component VO_2 thin film samples were abbreviated as V-A, V-R, V-C, V-M and TiO_2 thin film samples were T-A, T-R, T-C, T-M.

Spinodal decomposition is illustrated on a phase diagram (Fig. 1). Usually, phase separation occurs whenever a material transforms into the thermodynamically unstable regions. The borderline of the unstable region to the stable region, often called the binodal curve, was first reported in TVO by Zamma and Ueda in 1998[19] from calculations based on the common tangent construction of the free-energy diagram. Below the bimodal curve, there is a spinodal region, which was re-plotted from the literature data obtain from annealing experiments on the crystalline solid solution of $Ti_{0.4}V_{0.6}O_2$ at four temperatures (200, 300, 400 and 500 °C)[19,30]. For compositions within the spinodal, a homogeneous solution is unstable against infinitesimal fluctuations in density or composition[31].

It can be stated from Fig. 1 that, to reach the spinodal region, the material must cross the binodal region. Often phase separation occurs *via* nucleation and growth during the transition, and hence, spinodal decomposition cannot be observed. To avoid this scenario, a very fast transition by fast quenching is required to move the solid solution from the stable region to the spinodal region. This means spinodal decomposition needs rapidly quenching from high temperature (usually above 1000 °C) and post-annealing at the decomposition temperature. So far, this approach has been used in various spinodal systems[15,16,19,20], and the combination of quenching (above 700 °C) with annealing (500 °C) method (Q-A) has been proven to be efficient in our TVO system (see Supplementary Fig. S1). With respect to our magnetron sputtering technique, the fast quenching from high temperature is not suitable since both the substrates and the thin films could easily fracture upon quenching. Therefore, to ensure the composition stability and uniformity of amorphous films, we first propose a two-step approach, namely, the room temperature sputtering-annealing (RTS-A) approach in our TVO system[29], the schematic diagram of which is presented in Fig. S1. In our RTS-A route, spinodal decomposition is realized by directly annealing the amorphous TVO films, instead of high temperature and fast quenching.

Thin film composition was determined by XPS analysis (Fig. S2), the molar ratio of Ti to V is 0.33 for all the samples, and hence the composition can all be written as $Ti_{0.25}V_{0.75}O_2$. The composition ($Ti_{0.25}V_{0.75}O_2$) and the annealing temperature (500 °C) of the thin film are illustrated by the vertical and horizontal red dashed lines in Fig. 1, respectively. At the crosspoint, the final decomposed phases should be $Ti_{0.18}V_{0.82}O_2$ (V-rich) phase and the $Ti_{0.49}V_{0.51}O_2$ (Ti-rich) phase.

Researches[32–34] have found that the epitaxial growth of VO_2 and TiO_2 on sapphire substrates has different out-of-plane orientations in terms of the sapphire type, as follows:

A-sapphire: (101) VO_2(R)//(11–20) Al_2O_3, (101) TiO_2(R)//(11–20) Al_2O_3;
R-sapphire: (101) VO_2(R)//(1–102) Al_2O_3, (101) TiO_2(R)//(1–102) Al_2O_3;
C-sapphire: (100) VO_2(R)//(0001) Al_2O_3, (100) TiO_2(R)//(0001) Al_2O_3;
M-sapphire: (001) VO_2(R)//(10-10) Al_2O_3, (001) TiO_2(R)//(10-10) Al_2O_3.

Confirmed by XRD results (Fig. S3), spinodal decomposition samples share the same orientations with the single component ones, thus we achieve different decomposition modes. Note that both the Ti-rich and V-rich peaks are located between the peak of pure VO_2 and that of TiO_2, the composition of the separated phases are V-doped TiO_2 (Ti-rich phase) and Ti-doped VO_2 (V-rich phase), respectively.

Standard lattice parameters of rutile TiO_2 are $a = 4.582$, $c = 2.953$ (PDF: 78-1510), and of tetragonal VO_2 are $a = 4.554$, $c = 2.8557$ (PDF: 79-1655). The lattice mismatch in TVO system is 0.61% along the a axis and 3.3% along the c axis. In this case, spinodal decomposition modulation in the TVO system should occur along the c axis to minimize the elastic strain energy at the interface. The expected multilayers should be parallel to the (001) plane of TVO. This hypothesis is confirmed in TVO bulk crystals where spinodal decomposition occurs only for hkl reflections with $l \neq 0$[20]. Similarly, spinodal decomposition occurs only along the c axis, i.e., [001] direction in the TiO_2/SnO_2 system[15,35]. Combined with the XRD results, we can infer the direction of decomposed multilayers will be slanted with respect to the substrate for SD-A and SD-R, perpendicular to the substrate for SD-C, and parallel to the substrate for SD-M. Schematic diagrams of the microstructure of the spinodally decomposed TVO thin films are shown in Fig. 2. Figure 2 also shows the cross-sectional EDS elemental mapping of Ti and V (originate from the STEM in Fig. S4), in high consistence with the schematic structures. The overall thickness of the TVO film was measured to be about 120 nm (Fig. S5), the thickness of Ti-rich layer is estimated to be ~20 nm(-Fig. S4). Detailed high-resolution TEM analyses are shown in Fig. S5.

Evolution of the separated phases during spinodal decomposition was monitored on SD-M samples annealed for different annealing time, as shown in Fig. 3. Since there is no thermodynamic barrier to the reaction inside the spinodal region (Fig. 1), spinodal decomposition proceeds solely *via* diffusion mechanism, and the schematic diagram of the element (Ti or V) content fluctuation evolution is shown in Fig. 3(a). It is a sinusoidal wave curve, the amplitude increases along with annealing time and the amplitude is limited by the composition of original solid solution. The film thickness of amorphous sample (A-M) is about 120 nm, investigated by TEM (Fig. 3(b)) and the film surface is flat. TEM proves that A-M was predominantly amorphous since only few crystalline domains are present. Moreover, in HRTEM of Fig. 3(c), there is a pronounced epitaxial crystalline layer of ~10 nm forms in the interface between the substrate and TVO film. The interplanar crystal spacing is measured to be 2.9 Å, matching well with the $2d$ value calculated from XRD (002) peaks of sample C-M (64.45°, $d = 1.46$ Å) in Fig. S3(d). It is reasonable to state that the sapphire substrate is effective in promoting epitaxial growth and the epitaxial thin layer can act as seeds of the two separated phases in the following annealing process.

EDS elemental mapping, and EDS line scanning are shown in Fig. 3(d),(e) and (f) for annealing times of 1 h, 5 h, 10 h, respectively (originate from the STEM images in Fig. S6). The images of each EDS line scan, which starts from the interface between the substrate and TVO and ends at the surface of TVO film, agree well with the schematic diagrams in Fig. 3(a), supporting the diffusional scenario. At the beginning of annealing (1 h, Fig. 3(d)), the as-grown film is a homogeneous solid solution and only little fluctuation can be observed. With the annealing, fluctuations grow until individual phases can be identified (5 h, Fig. 3(e)), but the phase separation is incomplete and appears to be wavy lamellar structures at this stage. After sufficient annealing (over 10 h, Fig. 3(f)), the final equilibrium of phase separation with relatively sharp interface structure has been established. The final phase is stable with extending the annealing time at the fixed annealing temperature, because compared with the 10 h annealed sample, the longer time annealed (20 h) one displays similar XRD intensity (Fig. S7), similar transmittance spectra (Fig. S8(a and b)), and similar hysteresis loops (Fig. S8(c)).

For application purposes, spinodally decomposed TVO thin films (SD-A, SD-R, SD-C, SD-M) are regarded as VO_2 and TiO_2 multilayer thin films. Based on the semiconductor-metal transition of VO_2, those thin films are expected to be utilized as smart windows[27]. The vis-near-infrared transmittance spectra of the composite films were characterized at 20 °C (before phase transition) and 90 °C (after phase transition) to determine their optical modulation capability, as shown in Fig. 4(a–d). Transmittance spectra of single VO_2 samples (V-A, V-R, V-C, V-M) are also shown for comparison. The application of VO_2 for smart windows relies on the enhancement in both luminous transmittance (T_{lum}) and solar modulating ability (ΔT_{sol}), which are determined using the following equation[36]:

$$T_\rho = \int \psi_\rho(\lambda) T(\lambda) d\lambda / \int \psi_\rho(\lambda) d\lambda \quad (1)$$

$$\Delta T = \Delta T_{sol,20^\circ C} - \Delta T_{sol,90^\circ C} \quad (2)$$

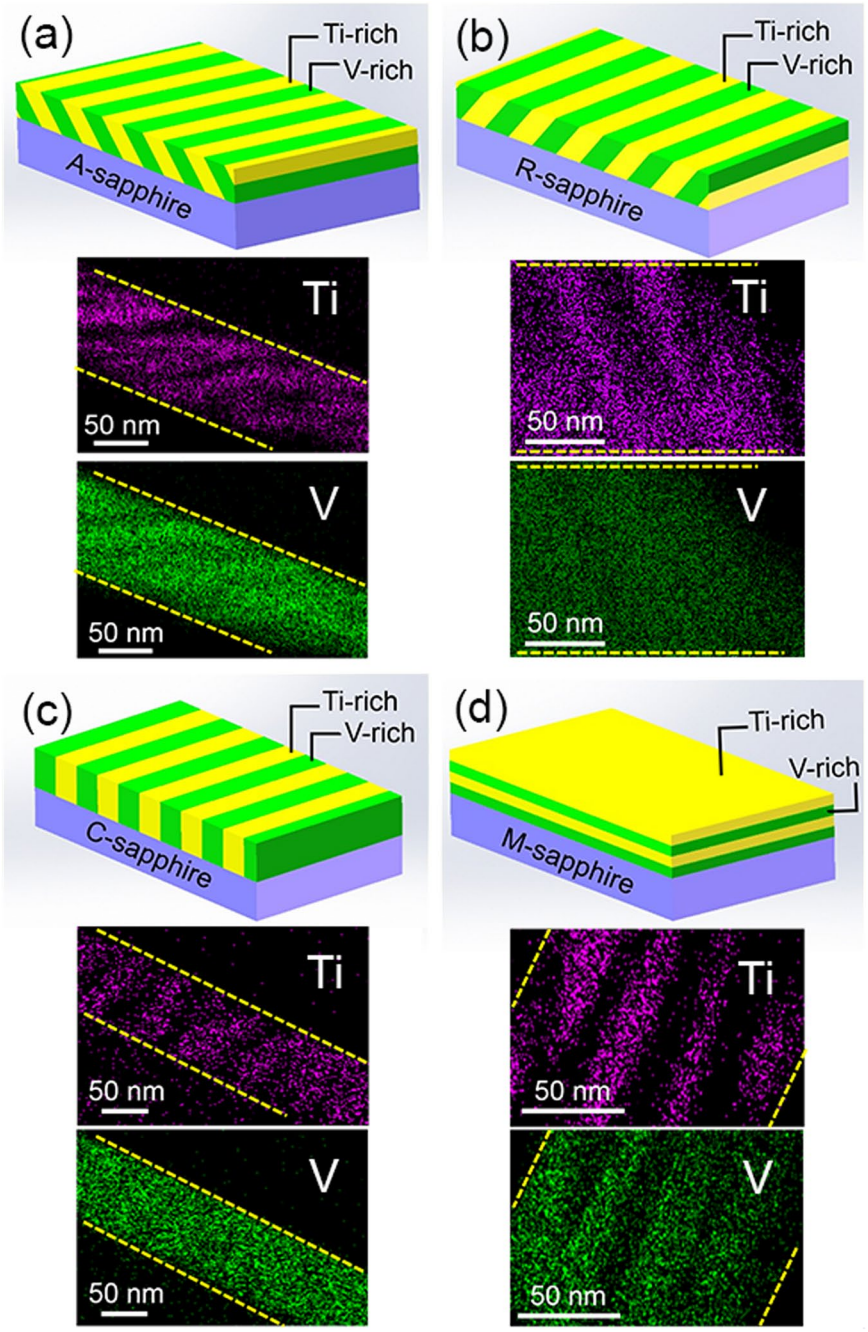

Figure 2. Schematic diagrams of the microstructure of spinodally decomposed TVO for (**a**) SD-A, (**b**) SD-R, (**c**) SD-C and (**d**) SD-M, and the related EDS elemental mapping (Ti and V) analyses of the selected area in Fig. S4.

where $T(\lambda)$ is the transmittance at wavelength λ, ρ denotes *lum* or *sol* for calculations, ψ_{lum} is the standard efficiency function for photopic vision, and ψ_{sol} is the solar irradiance spectrum for an air mass of 1.5 (corresponding to the sun standing 37° above the horizon). The optical features of samples are summarized in Table 1.

In Fig. 4(a–d) and Table 1, each spinodally decomposed TVO film (SD-A, SD-R, SD-C, SD-M) displays thermochromic properties, compare with the optical properties of the recently reported VO_2-based thermochromic films prepared by magnetron sputtering (listed in Table S2), one can see that all the film can potentially be applied as smart coating material. However, compared to the single VO_2, the relative tendency is not uniform across the four types. Comparing SD-A to V-A, the T_{lum} remains constant, while the ΔT_{sol} increases significantly from 6.1% for V-A to 9.6% for SD-A. The transmittance difference of typical wavelength of 2000 nm ($\Delta T_{2000\,nm}$) is measured as 46.4% for V-A and 51.7% for SD-A. For SD-R relative to V-R, and both T_{lum} and ΔT_{sol} decrease while $\Delta T_{2000\,nm}$ increases. This indicates that the Ti-rich coatings slightly increase the total transmittance, but lead to a red shift of the absorption edge in Fig. 4(b), consistent with the function of TiO_2 coatings in VO_2 based thin films[37]. SD-C exhibits an increase in T_{lum}, but more obvious decrease in ΔT_{sol} compared to V-C (Fig. 4(c)). The change

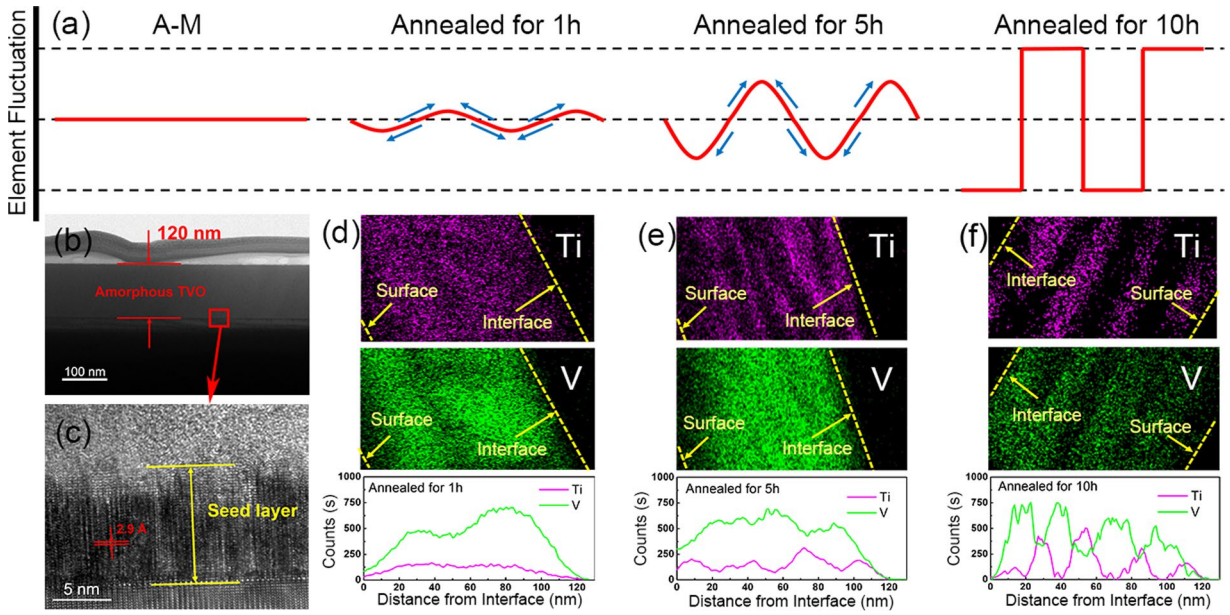

Figure 3. (**a**) Schematic diagram of element (Ti or V) content fluctuation in phase separation evolution progress. (**b**) TEM image of A-M sample. (**c**) High resolution TEM image of the select red square area in image (**b**). (**d**–**f**) EDS elemental mapping of the selected area (white square in Fig. S6) and line scanning of selected line (yellow line in Fig. S6) analyses for (**e**) sample annealing for 1 h, (**f**) sample annealing for 5 h, (**g**) sample annealing for 10 h. All the EDS line scanning images begin from the interface between TVO film and substrate and end at the surface of TVO film.

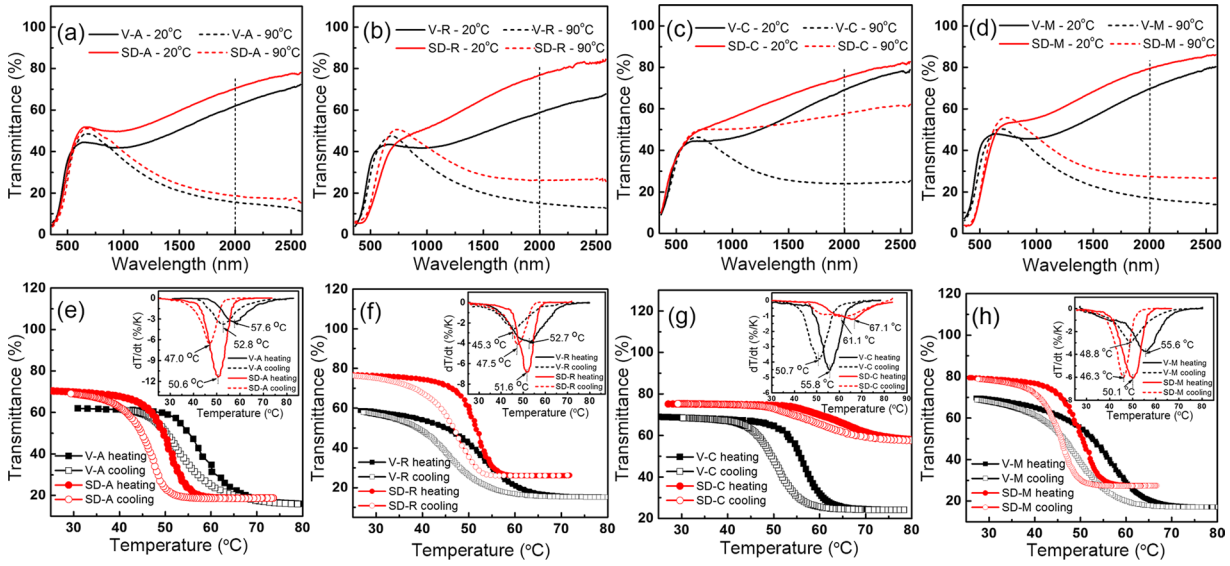

Figure 4. (**a**–**d**) Vis-near-infrared transmittance spectra at 20 °C and 90 °C of samples (**a**) V-A, SD-A, (**b**) V-R, SD-R, (**c**) V-C, SD-C, (**d**) V-M, SD-M. (**e**–**h**) emperature-varied transmittance hysteresis loops of samples (**e**) V-A, SD-A, (**f**) V-R, SD-R, (**g**) V-C, SD-C, (**h**) V-M, SD-M. Insets are the first-order differential curves of transmittance to temperature (dT/dt).

is reasonable because the perpendicular orientation of the microscopic structure causes incomplete coverage of the V-rich layers on the substrate thus increases the total transmittance for the higher transparent property of Ti-rich layer[29], and lowers the thermochromic functional area. SD-M displays relatively high thermochromic performance with T_{lum} of 32.3% at 20 °C, 35.9% at 90 °C, ΔT_{sol} of 6.6%, and $\Delta T_{2000\,nm}$ of 51.9%. These data are slightly lower than those of V-M. For the relatively high-level Ti-doping in V-rich layers, the total transmittance improvement and red shift phenomena are similar to SD-R and SD-A. More detailed band gap calculation data are discussed and shown in Fig. S9.

Sample	T_{lum} (%)		T_{sol} (%)		ΔT_{sol} (%)	ΔT_{2000nm} (%)	$T_{c\text{-}heating}$ (°C)	$T_{c\text{-}cooling}$ (°C)	ΔT_c (°C)
	20 °C	90 °C	20 °C	90 °C					
V-A	40.7	40.0	40.5	34.4	6.1	46.4	57.6	52.8	4.8
SD-A	42.7	39.7	45.4	35.8	9.6	51.7	50.6	47.0	3.6
V-R	39.8	38.7	39.6	33.0	6.6	43.7	52.7	45.3	7.4
SD-R	22.7	29.1	38.8	34.1	4.7	50.5	51.6	47.5	4.1
V-C	41.1	40.7	43.3	35.8	7.5	45.0	55.8	50.7	5.1
SD-C	41.5	42.1	48.6	45.3	3.3	17.6	67.1	61.1	6.0
V-M	45.0	41.8	44.5	36.5	8.0	52.5	55.6	48.8	6.8
SD-M	32.3	35.9	44.7	38.1	6.6	51.9	50.1	46.3	3.8

Table 1. Optical properties of single VO_2 samples and spinodal decomposition samples.

As shown in Fig. 4(e–h), the hysteresis loops were measured at 2000 nm. Phase-transition temperatures of heating lines ($T_{c\text{-}heating}$) and cooling lines ($T_{c\text{-}cooling}$) are obtained from the peak value of the first-order differential curves (dT/dt), respectively[38]. Usually, $T_{c\text{-}heating}$ is often used to represent the phase-transition temperature (T_c). The hysteresis loop width (ΔT_c) is estimated through $\Delta T_c = T_{c\text{-}heating} - T_{c\text{-}cooling}$ (see the insets of Fig. 4(e–h) and Table 1).

The T_c of the VO_2 single crystal should be ~68 °C[39], but our single VO_2 samples are decreased to: 57.6 °C for V-A, 52.7 °C for V-R, 55.8 °C for V-C, and 55.6 °C for V-M. The decrease in T_c is ascribed mainly to the stress arising from ion bombardment during the deposition process and the mismatch in coefficient of thermal expansion between VO_2 film and sapphire. For spinodally decomposed TVO films, only SD-C displays an increase in T_c, others show decrease in T_c. Jin *et al*. have indicated that the T_c reduction of VO_2 film results mainly from doping and/or lattice stress[37]. Researches have found that the T_c value of VO_2 would slightly increase by Ti doping[40,41], which seems not to be the main influence factor of the variation. Generally, for lattice stress in VO_2-based thermochromic multilayer film, the anisotropic compression pressure along the *c* axis of VO_2 layer is the most effective strain, compressive stress along *c* axis causes the incerease in T_c, while the tensile stress decreases T_c. As we discussed above, spinodal decomposition in our TVO system occurs along the *c* axis to minimize the elastic strain energy. Since the *a* axis of TiO_2 ($a = 4.582$, PDF: 78-1510) is larger than VO_2, ($a = 4.554$, PDF: 79-1655), the *a* axis of V-rich layer should be under tensile stress while the *c* axis is under compressive stress in the V-rich phase, causing the reduction in T_c in SD-A, SD-R, and SD-M samples. For the V-rich layer in SD-C, the same influence from Ti-rich also exist. Nevertheless, since the orientation relationship between V-rich layer and the substrate is (100) VO_2(R)//(0001) Al_2O_3, and the spinodally decomposed layers are perpendicular to the substrate, *b* axis and *c* axis of VO_2(R) (tetragonal, $a = 4.55$, $c = 2.86$) are extended for the larger lattice paremeter of Al_2O_3(hexagonal, $a = 4.75$), schematic illustration of heteroepitaxial relationship and tensile stress in VO_2 of VO_2/Al_2O_3 interface could be found in our previous work[34]. Put these two competitive factors together, the *c* axis of V-rich layer is suffered tensile stress in SD-C sample at length.

Ladd has reported that anisotropic compression along *c* axis could theoretically reduce T_c by −12 °C/GPa[42]. From Table 1, the reduction of SD-A is 7.0 °C, SD-R is 1.1 °C, and SD-M is 5.5 °C, thus the anisotropic pressure is estimated as ≥0.58 GPa in SD-A, ≥0.1 GPa in SD-R, and ≥0.46 GPa in SD-M. Thus, we can state that spinodal decomposition is a new route to achieve huge anisotropic stress. Internal stress is of importance for high-frequency response VO_2 applications, and this is confirmed by the reduction in hysteresis loop width (ΔT_c) of SD-A, SD-R, and SD-M (Table 1).

Moreover, to evaluate the stability of spinodally decomposed films, durability experiments have been performed on V-M and SD-M, with the condition of a constant-temperature 60 °C and relative humidity of 90%, shown in Fig. S10. Results shown the thermochromism nearly vanishes after about 15 days' treatment for V-M and 36 days for SD-M, pronounced the improvement in durability with spinodal decomposition. For a comparison, protective Al_2O_3 coating can be thermochromic only for 7 days[43], while WO_3 coatings are durable even after 20 days[44].

Conclusions

Fabrication of self-assembled lamella multilayer VO_2-TiO_2 thin films was realized by a two-steps approach of room temperature magnetron sputtering - post annealing *via* spinodal decomposition mechanism. The spinodally decomposed TVO film has been achieved on different sapphire substrates (A-plane (11–20) sapphire, R-plane (1–102) sapphire, C-plane (0001) sapphire, M-plane (10-10) sapphire substrates). All decomposed films display nano-scaled multilayer structures with well-ordered alternating Ti-rich and V-rich parallel layers, while the multilayered TVO structure and substrate have different orientations. The decomposed films tend to be slanted on A- and R-sapphire, perpendicular on C-sapphire, and parallel on M-sapphire. The spinodal decomposition is governed by a diffusional mechanism.

The annealing at 500 °C for 10 h can lead to a complete phase separation via our RTS-A method. All spinodally decomposed TVO films display thermochromic properties, and hence, our new technique has a high potential to be applied on smart coatings. The decomposed films on A-, R-, and M-sapphire also show both the reduced transition temperature and the narrowed hysteresis loop of the thermochromic V-rich layer. The spinodally decomposed TVO thin film bears anisotropic stress, and thus, it is promising to be utilized in optical switching. Moreover, the spinodally decomposed films display significantly better durability than VO_2 thin film. These

self-assembled multilayer-structures and outstanding regulating optical properties indicate that spinodal decomposition is an ideal approach for fabricating VO_2-based smart windows.

Methods

Amorphous TVO thin films (A-A, A-R, A-C, A-M) were first deposited by magnetron sputtering (ULVAC, ACS-4000-C4) on A-sapphire, R-sapphire, C-sapphire, M-sapphire substrates respectively, and then annealed for spinodal decomposition. The deposition of these amorphous TVO samples was carried out by co-sputtering from a VO_2 ceramic target at 70 W dc power and a TiO_2 ceramic target at 100 W rf power at room temperature with Ar and O_2 flow of 39 and 1 sccm, respectively. Representative spinodal decomposition (SD) samples (SD-A, SD-R, SD-C, SD-M) were then obtained by annealing the amorphous samples at 500 °C for 10 h at 1 mTorr. For comparison, crystalline solid solution TVO (C-A, C-R, C-C, C-M) were prepared under nearly identical conditions as the amorphous samples, except that the substrate temperature was kept at 450 °C while sputtering. Single component VO_2 thin film samples (V-A, V-R, V-C, V-M) and TiO_2 thin film samples (T-A, T-R, T-C, T-M) were prepared at 450 °C by alternatively DC sputtering a VO_2 ceramic target at 70 W and RF sputtering a TiO_2 ceramic target at 100 W. A schematic diagram of the preparation processes can be found in Fig. S1(a).

X-ray photoemission spectroscopy (XPS) analysis was conducted on ThermoFisher ESCAlab250 to detect the elementary composition and content of TVO. Thin film X-ray diffraction (XRD) analysis was carried out on a Rigaku Ultima IV diffractometer with Cu Kα radiation ($\lambda = 1.5418$ Å) using the θ-2θ scanning model. Transmission electron microscopy (TEM) observations were carried out with the electron microscope (FEI, TECNAI G^2 F20) equipped with an EDS analyzer (OXFORD, X-Max^N). The optical transmittance of the films in the wavelength range from 350 nm to 2600 nm at 20 °C and 90 °C was measured using a UV-Vis spectrophotometer (HITACHI, UV-4100). The temperature was measured precisely with a temperature sensor in contact with the surface of films and controlled by a temperature controlling unit.

In addition, summary of the acronyms in this manuscript has been listed at the last of the supporting information in Table S3.

Data availability statement. All data generated or analysed during this study are included in this published article and its Supplementary Information files.

References

1. MaCmanus-Driscoll, J. L. *et al*. Strain control and spontaneous phase ordering in vertical nanocomposite heteroepitaxial thin films. *Nat. Mater.* **7**, 314–320 (2008).
2. Yabu, H., Koike, K., Motoyoshi, K., Higuchi, T. & Shimomura, M. A Novel Route for Fabricating Metal-Polymer Composite Nanoparticles with Phase-Separated Structures. *Macromol. Rapid Commun.* **31**, 1267–1271 (2010).
3. Zheng, H. *et al*. Multiferroic $BaTiO_3$-$CoFe_2O_4$ nanostructures. *Science* **303**, 661–663 (2004).
4. Harrington, S. A. *et al*. Thick lead-free ferroelectric films with high Curie temperatures through nanocomposite-induced strain. *Nat. Nanotechnol.* **6**, 491–495 (2011).
5. Young, K. L. *et al*. Using DNA to Design Plasmonic Metamaterials with Tunable Optical Properties. *Adv. Mater.* **26**, 653–659 (2014).
6. Yang, S. *et al*. Feedback-driven self-assembly of symmetry-breaking optical metamaterials in solution. *Nat. Nanotechnol.* **9**, 1002–1006 (2014).
7. Yao, J. *et al*. Optical negative refraction in bulk metamaterials of nanowires. *Science* **321**, 930–930 (2008).
8. Nan, C. W. & Jia, Q. X. Obtaining ultimate functionalities in nanocomposites: Design, control, and fabrication. *Mrs Bull.* **40**, 719–723 (2015).
9. MacManus-Driscoll, J. L., Suwardi, A. & Wang, H. Composite epitaxial thin films: A new platform for tuning, probing, and exploiting mesoscale oxides. *Mrs Bull.* **40**, 933–942 (2015).
10. Chen, Z. *et al*. Self-Assembled, Nanostructured, Tunable Metamaterials via Spinodal Decomposition. *ACS nano* **10**, 10237–10244 (2016).
11. Cahn, J. W. On Spinodal Decomposition. *Acta Metall. Mater.* **9**, 795–801 (1961).
12. Cahn, J. W. & Hilliard, J. E. Free Energy of a Nonuniform System .1. Interfacial Free Energy. *J. Chem. Phys.* **28**, 258–267 (1958).
13. Guiton, B. S. & Davies, P. K. Nano-chessboard superlattices formed by spontaneous phase separation in oxides. *Nat. Mater.* **6**, 586–591 (2007).
14. Padurow, N. N. Mischbarkeit Im System Rutil-Zinnstein. *Naturwissenschaften* **43**, 395–396 (1956).
15. Shuichi, A., Kenji, M., Ko-ichi, K. & Toshinobu, Y. Hirano, S.-i., Gas-Sensing Properties of Spinodally Decomposed (Ti, Sn)O_2 Thin Films. *J. Am. Ceram. Soc.* **82**, 225–228 (1999).
16. Chaisan, W., Yimnirun, R., Ananta, S. & Cann, D. P. The effects of the spinodal microstructure on the electrical properties of TiO_2–SnO_2 ceramics. *J. Solid State Chem.* **178**, 613–620 (2005).
17. Schultz, A. H. & Stubican, V. S. Separation of Phases by Spinodal Decomposition in Systems Al_2O_3-Cr_2O_3 and Al_2O_3-Cr_2O_3-Fe_2O_3. *J. Am. Ceram. Soc.* **53**, 613–616 (1970).
18. Chen, J., Tian, Q. & Virkar, A. V. Phase-Separation in the Sic-Aln Pseudobinary System - the Role of Coherency Strain-Energy. *J. Am. Ceram. Soc.* **75**, 809–821 (1992).
19. Hiroi, Z., Hayamizu, H., Yoshida, T., Muraoka, Y. & Okamoto, Y. Yamaura, J.-i.; Ueda, Y., Spinodal Decomposition in the TiO_2–VO_2 System. *Chem. Mater.* **25**, 2202–2210 (2013).
20. Hiroi, Z., Yoshida, T., Yamaura, J. & Okamoto, Y. Spinodally decomposed nanostructures in a TiO_2–VO_2 crystal. *APL Mater.* **3**, 062508 (2015).
21. Yang, S. *et al*. Bottom-up approach toward single-crystalline VO_2-graphene ribbons as cathodes for ultrafast lithium storage. *Nano Lett.* **13**, 1596–601 (2013).
22. Dey, K. K. *et al*. VO_2 nanorods for efficient performance in thermal fluids and sensors. *Nanoscale* **7**, 6159 (2015).
23. O'Callahan, B. T. *et al*. Inhomogeneity of the ultrafast insulator-to-metal transition dynamics of VO_2. *Nat. Commun.* **6**, 6849 (2015).
24. Zhang, H. T. *et al*. Wafer-scale growth of VO_2 thin films using a combinatorial approach. *Nat. Commun.* **6**, 8475 (2015).
25. Sun, G. *et al*. Low-temperature deposition of VO_2 films with high crystalline degree by embedding multilayered structure. *Solar Energy Materials and Solar Cells* **161**, 70–76 (2017).
26. Tazawa, M., Yoshimura, K., Jin, P. & Xu, G. Design, formation and characterization of a novel multifunctional window with VO_2 and TiO_2coatings. *Appl. Phys. A: Mater. Sci. Process.* **77**, 455–459 (2003).
27. Zheng, J., Bao, S. & Jin, P. TiO_2(R)/VO_2(M)/TiO_2(A) multilayer film as smart window: Combination of energy-saving, antifogging and self-cleaning functions. *Nano Energy* **11**, 136–145 (2015).

28. Zhou, Y., Cai, Y., Hu, X. & Long, Y. Temperature-responsive hydrogel with ultra-large solar modulation and high luminous transmission for "smart window" applications. *J. Mater. Chem. A* **2**, 13550 (2014).
29. Sun, G. *et al*. Self-Assembled Multilayer Structure and Enhanced Thermochromic Performance of Spinodally Decomposed TiO_2–VO_2Thin Film. *ACS Appl. Mater. Interfaces* **8**, 7054–7059 (2016).
30. Hiroi, Z. Structural instability of the rutile compounds and its relevance to the metal–insulator transition of VO_2. *Prog. Solid State Chem.* **43**, 47–69 (2015).
31. Jones, R. A. L. *Soft Condensed Matter*. Oxford University Press: 2004.
32. Li, J. & Dho, J. Controlling metal–insulator transition in the hetero-epitaxial VO_2/TiO_2 bilayer grown on Al_2O_3. *J. Cryst. Growth* **312**, 3287–3291 (2010).
33. Zhao, Y. *et al*. Structural, electrical, and terahertz transmission properties of VO_2 thin films grown on c-, r-, and m-plane sapphire substrates. *J. Appl. Phys.* **111**, 053533 (2012).
34. Sun, G. *et al*. Structure and enhanced thermochromic performance of low-temperature fabricated VO_2/V_2O_3 thin film. *Appl. Phys. Lett.* **109**, 143903 (2016).
35. Stubican, V. S. & Schultz, A. H. Spinodal Decomposition in System TiO_2-SnO_2. *J. Am. Ceram. Soc.* **51**, 290–291 (1968).
36. Gao, Y. *et al*. Enhanced chemical stability of VO_2 nanoparticles by the formation of SiO_2/VO_2 core/shell structures and the application to transparent and flexible VO_2-based composite foils with excellent thermochromic properties for solar heat control. *Energy Environ. Sci.* **5**, 6104 (2012).
37. Jin, P., Xu, G., Tazawa, M. & Yoshimura, K. Design, formation and characterization of a novel multifunctional window with VO_2 and TiO_2coatings. *Appl. Phys. A: Mater. Sci. Process.* **77**, 455–459 (2003).
38. Chen, C. *et al*. VO_2 multidomain heteroepitaxial growth and terahertz transmission modulation. *Appl. Phys. Lett.* **97**, 211905 (2010).
39. Morin, F. J. Oxides Which Show a Metal-to-Insulator Transition at the Neel Temperature. *Phys. Rev. Lett.* **3**, 34–36 (1959).
40. Nishikawa, M., Nakajima, T., Kumagai, T., Okutani, T. & Tsuchiya, T. Ti-Doped VO_2 Films Grown on Glass Substrates by Excimer-Laser-Assisted Metal Organic Deposition Process. *Jpn. J. Appl. Phys.* **50**, 01BE04 (2011).
41. Chen, S., Liu, J., Wang, L., Luo, H. & Gao, Y. Unraveling Mechanism on Reducing Thermal Hysteresis Width of VO_2 by Ti Doping: A Joint Experimental and Theoretical Study. *J. Phys. Chem. C* **118**, 18938–18944 (2014).
42. Ladd, L. A. & Paul, W. Optical and Transport Properties of High Quality Crystals of V_2O_4 near Metallic Transition Temperature. *Solid State Commun.* **7**, 425–428 (1969).
43. Ji, Y. X., Li, S. Y., Niklasson, G. A. & Granqvist, C. G. Durability of thermochromic VO_2 thin films under heating and humidity: Effect of Al oxide top coatings. *Thin Solid Films* **562**, 568–573 (2014).
44. Long, S. *et al*. Thermochromic multilayer films of $WO_3/VO_2/WO_3$ sandwich structure with enhanced luminous transmittance and durability. *RSC Adv.* **6**, 106435–106442 (2016).

Acknowledgements

This study was financially supported by the National Natural Science Foundation of China (NSFC, 51572284), and the Shanghai Sailing Program (17YF1429800). And the authors are grateful for The Youth Innovation Promotion Association, Chinese Academy of Sciences (No. 2018288).

Author Contributions

G.S. wrote the main manuscript text under guidance of X.C. and P.J. Y.Y. and X.G. contributed to the result discussion. S.L., N.L. and R.L. assisted for sample synthesis and basic characterization. G.S. conceived the experiments under supervision of H.L. and P.J. X.C. and P.J. planned and supervised this study. All authors participated in discussions and manuscript writing.

Additional Information

Supplementary information accompanies this paper at https://doi.org/10.1038/s41598-018-23412-4.

Competing Interests: The authors declare no competing interests.

Publisher's note: Springer Nature remains neutral with regard to jurisdictional claims in published maps and institutional affiliations.